



Transition metal decorated Ferrosferric oxide (Fe_3O_4): An expeditious catalyst for photodegradation of Carbol Fuchsin in environmental remediation

Prashant Bhimrao Koli^{a,*}, Kailas Haribhau Kapadnis^b, Uday Gangadhar Deshpande^a

^a Research Centre in Chemistry and PG Department of Chemistry, Pratap College, Amalner, Affiliated to KBC-NMU, Jalgaon, MH, 425401, India

^b Research Centre in Chemistry and PG Department of Chemistry, Loknete Vyankatrao Hiray Arts, Science and Commerce College, Panchavati, Nashik, Affiliated to SPPU, Pune, MH, 422003, India



ARTICLE INFO

Keywords:

Ferrosferric oxide
Carbol Fuchsin toxicity
Effluent treatment
XPS
Zeta potential
Photocatalysis

ABSTRACT

In this research, we report the removal of Carbol Fuchsin dye by using doped Ferrosferric oxide nanocatalyst. The nanocatalysts Fe_3O_4 and doped Fe_3O_4 was characterized by various methods. The structural properties of the prepared Fe_3O_4 doped Fe_3O_4 were investigated by using X-Ray Diffractometer (XRD), which confirmed the single-phase Fe_3O_4 nanoparticles. The surface, texture, morphology of nanoparticles was identified, from SEM. The crystal lattice confirmed from TEM. The magnetic property of Fe_3O_4 was confirmed by VSM analysis. The elemental composition of prepared pure and doped Ferrosferric oxide was confirmed by EDS study. The zeta potential was investigated for the stability of iron oxide nanoparticles. XPS spectrum of doped Fe_3O_4 was analysed to find the surface characteristics and elemental composition of doped Fe_3O_4 nanocatalyst. Here undoped Fe_3O_4 and doped Fe_3O_4 were comparatively investigated for the Carbol Fuchsin dye degradation study. Different parameters like initial catalyst dose, the effect of pH, contact time, dye concentration, effect of dopants, catalyst recycling have been studied to optimize degradation study. The optimum conditions for the removal of the Carbol Fuchsin dye are found to be initial concentration 20 mg/L, photocatalyst dose 8 gm/L, pH 8.0. In kinetics study, Pseudo First order kinetics has been investigated for both pure and doped Ferrosferric oxide catalyst. Almost 97% of dye degradation has been observed for doped iron oxide.

1. Introduction

In the modern civilized world, countless problems are associated with mankind due to unnecessary industrial and anthropological activities. Today the numerous problems associated with environment can be listed as pollution, population, production of toxic chemicals, toxic gases released by industries leads to pollution, mutagenic disorders due to the consumption of toxic substances, etc. [1,2]. Among these unnecessary activities the considerable effect on flora and fauna caused by water pollution. Although the scientist community working very hard to defeat this environmental problem. Till date the water and air pollution problems are not solved completely to clean the environmental hazards due these toxic chemical substances. [3,4].

From last couple of decades, there is huge enhancement in industries, modernization, and civilization. There is large demand from the complete universe is inside the garment section. Approximately 60% of cotton has been utilized by clothing industries for the

fabrication of colorful clothes. Largely the cotton, textile, paint, printing and textile industries utilizes thousands of colourful dyes to decorate the designing and beauty of cloths [5–7]. As majority of the dyes are very cheap as a result they're preferentially utilized by textile/paint industries for the coloring purpose. According to analysis and survey, the dyes utilized by the industries for coloring purpose are indiscriminately discharged into the flowing rivers or nearby coastal location [8]. Large number of industries utilized these coloring agents, chemical dyes etc. and flowing the waste dye water or coloring effluent into the water and accountable to make water pollution [9].

Every year from total production dyes/pigments nearly 11% of dyes are wasted as effluents, In Asian countries India sole produces nearly 64,000 tons of dyes every year and out of which 7040 tons are directly exuded into the environment as a pollutant. There are several categories of dyes such as basic dyes, acidic dyes, direct or substantive dyes, disperse dyes, azo dyes, reactive dyes, vat dyes, mordant dyes, sulphur dyes, etc. Miserable thing is almost 90% of dyes are water soluble and

* Corresponding author.

E-mail address: prashantkoli005@gmail.com (P.B. Koli).

<https://doi.org/10.1016/j.jece.2019.103373>

Received 11 June 2019; Received in revised form 12 August 2019; Accepted 16 August 2019

Available online 17 August 2019

2213-3437/ © 2019 Elsevier Ltd. All rights reserved.

they easily soluble in the water and become dangerous for aquatic life [10]. The major disadvantages of the dyes present in the water is disappearance of water transparency, utilization of more Dioxygen, elevation of biological oxygen demand, enhancement in chemical oxygen demand eventually disquiet the aquatic life. As per the previous reported study, most of the azo dyes and other class of dyes have aromatic structures present in flora and fauna can be the genesis for most of the severe, mutagenic and carcinogenic effect on the human health and amphibious life [11].

This environmental threat is can be solved by some common techniques such as photocatalysis, filtration, chemical degradation, adsorption, biodegradation, advanced oxidation process (AOP), microbial degradation in aerobic and anaerobic conditions where most of the dyes can be degraded in light-induced oxidative fading [12–14]. As there are a variety of dyes and hence dye degradation conditions may be varied from one type to another type. In several cases, basic dyes can be removed by adsorption via activated sludge, but these conditions are suitable for acidic dye because acidic dyes exhibit low adsorption values and they can be passed through activated sludge [15]. In addition to that microfiltration, continuous, and electrochemical color removal (ECR) methods are also helpful for dye/color removal and degradation. The ECR method occurs in a combination of adsorption and chemical reduction [16].

Besides these traditional methods of photocatalysis, now a day's doped semiconducting materials are very cheap and facile materials that can be employed for degradation or adsorption of dyes. Most of the researchers have been developed strategies for the synthesis nanomaterials, doped nanomaterials, nanocomposites, semiconductors decorated by CNT, Graphene, transition metal oxides (TMO) and inner transition metal oxides (ITMO), conducting polymers, magnetic semiconducting oxides, etc. variety of nanomaterials can be effectively employed for the photocatalysis purpose [17,18]. Class of spinel, inverse spinel, perovskites, and magnetite materials are very effectively employed for the adsorption and degradation purpose. The main purpose of the application of these materials for the degradation process is low-cost synthesis methods, no toxicity, good thermal stability, high surface area, good sorption capacity, and recycling properties [19].

Apart from above mentioned techniques and theories some more applicative strategies have been developed by researchers. The traditional or conventional activated sludge (CAS) has been utilized so far in many applications such as catalysis, waste water treatment etc. But in comparative study between CAS and nitrifying-enriched activated sludge (NAS) the hindmost is found to be more effective in the application such as improved filterability in membrane bioreactors, improved performance of effluent treatment, microbial population control, lowering of fouling. Thus in overall conclusions of NAS it can be summarized that the NAS based approach may be different but effective direction in the very current topic of investigation for researchers that is effluent treatment. Hence one should definitely approach to photocatalytic or adsorptive removal of dyes via NAS approach [20].

Among the popular methods of effluent treatment and environmental remediation the researchers are effectively utilizing the various materials for adsorptive removal of many organic pollutants, dyes, pesticides and some toxic metals such as Hg (II), Cr (VI), Cu (II) and Pb (II) etc. [21–23]. Adsorption is a worthy method for the catalytic application such as dye adsorption. Huge strategies have been adopted by the researchers in this case and comprehensively employed the adsorption models such as Langmuir, Freundlich, Sips isotherm model, Liu isotherm model, Redlich–Peterson Isotherm Model, Elovich–chemisorption kinetic adsorption model etc. Now a day's variety class of materials are employed by the researchers like polyacrylamide immobilized molybdenum disulphide composites effectively utilized as an adsorbent through mussel-inspired chemistry for Cu (II) ions removal. In most of the cases water is contaminated with toxic ions, to remove these ions via adsorption the MgAl-layered double hydroxide (LDH)

modified with polyethylene polyamine (PP) and tannic acid (TA) has been employed to improve the adsorption property of heavy metal ions. More expeditiously the magnetic graphene oxide material is also very effectively applied for the removal of metal ions via adsorption studies, in addition to above materials CNT functionalized by amine found to be excellent in the removal of some metals ions [24–29].

Mussel Chemistry is entirely novel and interesting adsorption method to increase the surface properties of the materials that can be helpful for adsorption studies. Most commonly the surface enhancement can be with the aid of binders, resins, pigments, solvents, and additives etc. The mussel surface properties originated from mussels (*M. californianus*) produces viscous liquids foot proteins (MFPS), which solidifies immediately and covered as coatings. [30–33]. In both the cases of Mussels and Squids the natural coating performance is depends on the composition of natural resin/binder. The researchers working on Mussel chemistry have identified that the mussel and squids contains essential amount of catecholic amino acid, 3,4 dihydroxyphenylalanine (DOPA) remains on the coatings. By taking the inspiration of the natural coatings researchers now aiming towards the synthesis of synthetic polymers derived from catechol, DOPA, O-quinones etc. All the materials derived from these materials have been effectively applied for the various application such as environmental adsorption, catalysis and biomedical applications etc. [34–36].

More recently magnetite or Ferroso-ferric oxide (Fe_3O_4) nanoparticles are reported to be very effective for the photocatalytic/adsorption purpose. These tiny nanomaterials are a worthy class of adsorbent which are ultrafine with the high surface area. The iron oxide is an excellent semiconductor possessing magnetic abilities that may be utilized in efficient separation with the supplement of superficial magnetic effect. The iron oxide possesses band gap in nearly 3 eV, but in several cases doping of transition metals or inner transition metal oxides may effectively reduce the band gap of iron oxide up to 2.3–2.5 eV. Hence the doped magnetite material becomes more effective for catalytic processes such as photocatalysis and adsorption phenomenon [37,38].

In the present investigation, we are reporting the rapid removal of Carbol Fuchsin dye

(CF dye) with the use of undoped and doped iron oxide (Fe_3O_4). The catalyst iron oxide is found to be very effective in photocatalytic removal of Carbol Fuchsin dye in slightly basic condition (pH = 8). Here comparative effects of undoped and doped iron oxide have been investigated. The effect of dopants Co^{2+} , Ni^{2+} has been investigated in comparison to the undoped iron oxide. The various parameters were optimized for photocatalysis, Kinetics of degradation and catalyst recycling has been reported.

2. Materials and methods

All the chemicals in this research used AR grade, purchased from Loba Chemie Mumbai and used without further purification. Chemicals used are Ferric chloride hexahydrate ($\text{FeCl}_3 \cdot 6\text{H}_2\text{O}$), ferrous chloride Tetra-hydrated ($\text{FeCl}_2 \cdot 4\text{H}_2\text{O}$), Nickel Chloride hexahydrate ($\text{NiCl}_2 \cdot 6\text{H}_2\text{O}$), Carbol Fuchsin dye, Cobalt chloride ($\text{CoCl}_2 \cdot 4\text{H}_2\text{O}$), Ammonia, double distilled water.

2.1. Synthesis of Ferrosferric oxide (Fe_3O_4) photocatalyst

Fe_3O_4 magnetic nanoparticles were prepared by the co-precipitation method. Complete precipitation of Fe_3O_4 was achieved under basic condition, by maintaining a molar ratio of $\text{FeCl}_2 \cdot 4\text{H}_2\text{O}$: $\text{FeCl}_3 \cdot 6\text{H}_2\text{O}$ as 1:2. In this study, $\text{FeCl}_2 \cdot 4\text{H}_2\text{O}$ and $\text{FeCl}_3 \cdot 6\text{H}_2\text{O}$ were dissolved in 80 ml distilled water with vigorous magnetic stirring. After stirring this solution heated up to 80 °C, then slowly added 1:1 ammonia solution by adjusting the pH of the solution up to 12. At this basic stage of the solution, complete precipitation of iron salts was found as iron hydroxide with the intense brown color of the solution. This iron hydroxide

precipitate was then washed with hot water and ethanol to make free from impurities. This precipitate was then allowed to Sonicate for 30 min, again it was washed and then dried in an oven for 1 h at 80 °C. Finally, the precipitate was transferred to silica crucible and ignited in a muffle furnace at 650 °C to form Fe₃O₄ nanoparticles

2.2. Synthesis of Co²⁺, Ni²⁺ incorporated Ferrosferric oxide (Fe₃O₄) photocatalyst

The in-situ doping concentration of Co²⁺ and Ni²⁺ (atomic weight 5%) was achieved by incorporating the cobalt chloride and nickel chloride salts into the Fe₃O₄ precursor solution during the synthesis of Ferrosferric oxide nanoparticles. For this the stoichiometric concentration in 1:2 mol of FeCl₂·4H₂O: FeCl₃·6H₂O was dissolved in 80 ml of distilled water, to this mix Iron solution, 5% atomic weight percentage of Co²⁺ and Ni²⁺ was added. Then slowly added 1:1 ammonia solution by adjusting the pH of the solution up to 12. At this basic stage of the solution, complete precipitation of iron salts was found as iron hydroxide, cobalt and nickel hydroxide with the black color of the solution. This precipitate was then allowed to Sonicate for 30 min, again it was washed and then dried in an oven for 1 h at 80 °C. Finally, the precipitate was transferred to silica crucible and ignited in a muffle furnace at 650 °C to form Co²⁺ and Ni²⁺ doped Fe₃O₄ nanoparticles [39].

2.3. Characterization techniques

The typical XRD pattern of the thick films of pure and doped nickel ferrite was recorded by using Bruker AXS D8 Advance GmbH (Germany), Bragg's scanning angle varying from 3-135°, Cu wavelength 1.54 Å. The surface morphology and characteristics of the material were analyzed by using a scanning electron microscope (SEM), model number S 4800 Type II High Technologies Corporation, Japan. The elemental composition and atomic weight percentage of all the elements in the pure and doped nickel ferrite films were investigated by using energy dispersive x-ray spectroscopy (EDAX), model number X Flash detector 5030 make Bruker AXS GmbH, Germany. Transmission electron microscope (TEM) was utilized to find out crystallinity, morphological features and crystal type of pure and doped ferrites, the model used for TEM analysis was CM200 make Philips with operating voltage 20-200 kV, resolution 2.4A₀ which can produce magnification up to 1000 000 ×. The sample of TEM was analyzed with the help of the copper grid. Additionally the doped iron oxide catalyst was characterized by X-ray photo electron spectroscopy (XPS), make Physical electronics model PHI 5000 VersaProbe III to investigate surface characteristics and material composition.

3. Results and discussions

3.1. XRD analysis

The XRD pattern of Ni²⁺, Co²⁺ decorated Fe₃O₄ and undoped Fe₃O₄ nanoparticles are shown in Fig. 2a and b from which formation of crystalline single phasic Fe₃O₄ was confirmed. Both these materials were analyzed by using X-ray diffraction technique with Bragg's scanning angle varying from 10-80°. The CuKα₁ radiations (wavelength 1.54Å) were used to generate the X-ray source. In the XRD spectrum as depicted in Fig. 1 from which the Bragg's reflection peaks can be assigned as the formation of Crystalline Fe₃O₄ with the cubic crystal lattice. The 2θ values of diffraction peaks obtained from XRD data for Fe₃O₄ material are 18.27, 30.09, 35.42, 43.05, 53.39, 56.94, 62.51, 70.92 and 86.70 The two-theta values can be assigned to the reflection of (111), (220), (311), (440), (422), (511), (440), (620) and (642) planes. The diffraction peaks mentioned above confirms the formation of Fe₃O₄ material. The average particle size was calculated by using Debye-Scherrer's formula. $[D = K\lambda/\beta \cos \theta]$, where D is

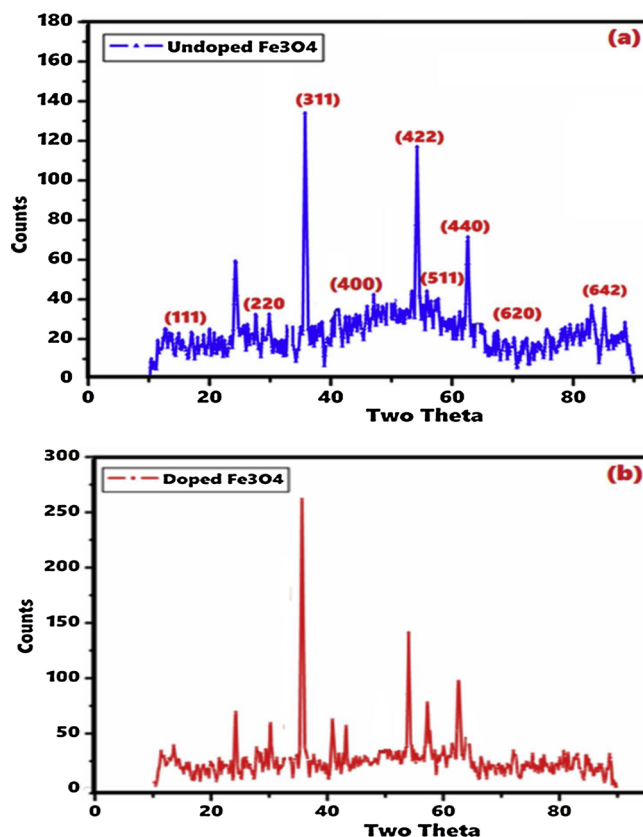


Fig. 1. (a) XRD pattern of undoped Fe₃O₄ nanoparticles. (b) XRD pattern Co²⁺, Ni²⁺ doped Fe₃O₄ nanoparticles.

average particle size, K is constant (0.9 to 1), β is full-width half maxima (FWHM) of a diffracted peak, θ is the angle of diffraction. The average particle size for undoped iron oxide was found to be 25.26 nm while for doped iron oxide it was 24.37 nm. The match scan data of Fe₃O₄ shows the formation of crystalline Fe₃O₄ nanoparticles with JCPDS number 00-019-0629 [40].

3.2. Scanning Electron microscopy

The structural, morphological and surface characteristics of Fe₃O₄ and modified Fe₃O₄ were investigated by means of scanning electron microscopy as depicted in Fig. 2. The SEM images of both pure and modified Fe₃O₄ shows the highly porous and cubic clusters of Ferrosferric oxide nanoparticles. The mapping image of pure Fe₃O₄ nanoparticles is ranging from 22.5 nm to 53.8 nm as shown in Fig. 3a. The various clusters and agglomerated nanoparticles with the uniform surface texture is can be observed from SEM images of pure and modified Fe₃O₄ nanoparticles. In the mapping images of modified Fe₃O₄, the nanoparticles with the various size ranging from 34.1 nm to 81.6 nm can be seen SEM images of modified Fe₃O₄. In both pure and modified Fe₃O₄, the various sized nanoparticles are found to be in good agreement with the XRD data. The various sized lumpy and agglomerated nanoparticles can be seen from the SEM images of both undoped and doped iron oxide. These agglomeration and lumps are useful in the heterogeneous catalysis particularly in the adsorption mechanism due to ease in providing the superior surface. Where the size of the average nanoparticles for both these materials is within the range of SEM data [41]. As the surface is the foremost factor in the catalysis, in the present research the surface area was enumerated by using the BET (Brunauer Emmett and Taller) method for spherical particles from SEM data using Eq. (2) represented in Table 1.

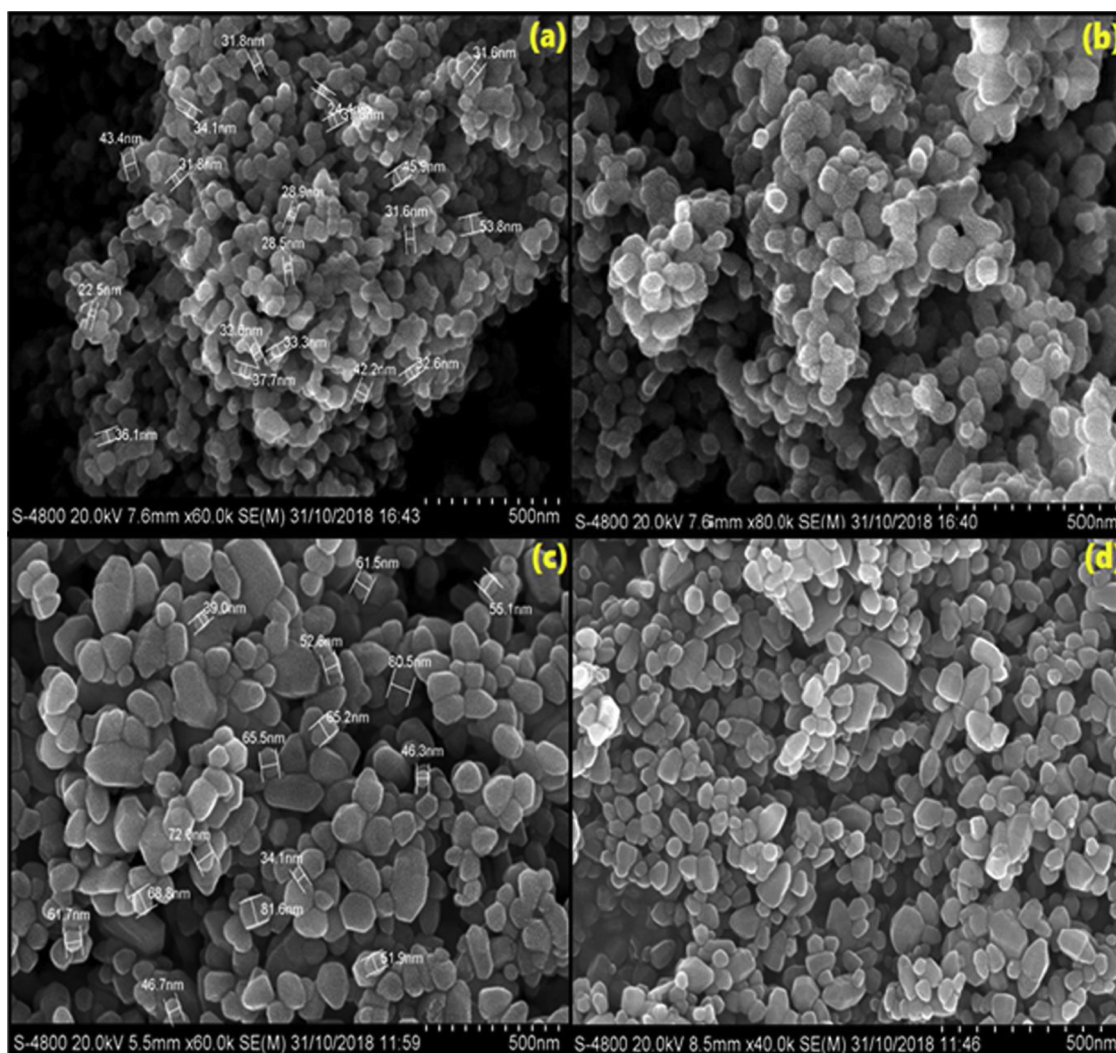


Fig. 2. (a),(b) Fe-SEM images of undoped Fe_3O_4 nanoparticles (c), (d). Fe-SEM image of Co^{2+} , Ni^{2+} doped Fe_3O_4 nanoparticles.

3.3. Particle size distribution using dynamic light scattering (DLS)

The particle size distribution (PSD) curves of the prepared catalysts i.e. Fe_3O_4 and Co^{2+} , Ni^{2+} doped Fe_3O_4 was analyzed with the help of dynamic light scattering. Where both these materials were dispersed in a dispersion medium like water. The PSD curves of both these materials are portrayed in Fig. 14a–b (Supplementary material File) as most of the physical and chemical properties are attributed to the size of the material, thus PDS is an excellent tool to investigate the particles distribution size. Here DLS was used to measure the particle size distribution of both these materials. In the present study, most of the nanoparticles are found in the range of 100 nm in case undoped Fe_3O_4 , while in case of doped Fe_3O_4 the nanoparticles were beyond the range of 100 nm, very few nanoparticles are observed in the range of 1000 nm. The smaller sized nanoparticles can be important in catalytic reaction. Both these materials ranged in a 100 nm thus being smaller in size nanoparticles are more significant to the photocatalysis study to provide more surface in photocatalysis [42,43].

3.4. Energy dispersive X-ray spectroscopy (EDS)

The elemental composition of both pure and modified Ferrosferric oxide (Fe_3O_4) was recorded with the aid of EDS. The EDS spectrum is as shown in Fig. 3a the sharp peak at 6.4 and 7.0 keV is attributed to

elemental iron. While in doped iron oxide the iron is resolution sharply at 6.4 keV and the dopant concentration of Co^{2+} and Ni^{2+} is observed at 6.9 and 7.0 keV on the EDS scale. The compositional data obtained from EDS analysis confirms the formation of Fe_3O_4 and modified Fe_3O_4 nanoparticles. In both the EDS spectrum no additional peaks of any impurity or elements were observed hence it can be concluded that prepared material is highly pure without any impurities [44]. The overall elemental composition of both undoped Ferrosferric oxide and doped Ferrosferric oxide nanomaterials is embedded in the EDS spectrum Fig. 3a and b.

3.5. High-resolution transmission electron microscopy (HR-TEM)

The crystal morphology of prepared Fe_3O_4 and Co^{2+} , Ni^{2+} doped Fe_3O_4 nanoparticles was observed by means of high-resolution transmission electron microscopy (HR-TEM) as reported in Fig. 4a–d. These both materials have cubic lattice according to the reported research. In the present investigation, both materials have cubic lattice is clearly observed from the TEM images with the range of 20–100 nm. In Fig. 4c and d the perfect spherical and oval-shaped nanoparticles are also present due use of precipitating agent during the synthesis of iron oxide nanoparticles, which may have worked as a reducing agent. The present TEM results of both pure and doped iron oxide are in good concurrence with previously reported results [45].

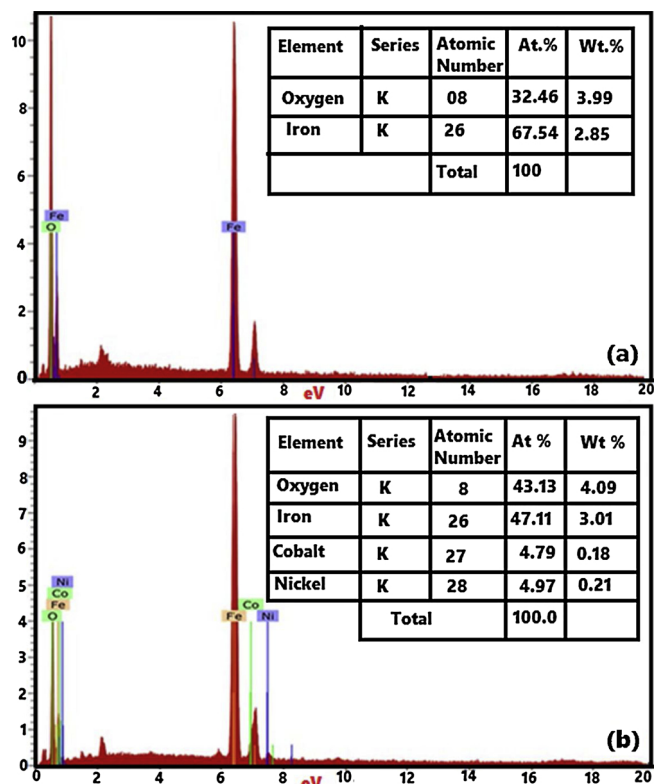


Fig. 3. (a) Energy dispersive X-ray spectrum of undoped Fe₃O₄ nanoparticles, (b) Energy dispersive X-ray spectrum of Co²⁺, Ni²⁺ doped Fe₃O₄ nanoparticles.

3.6. Magnetic study by VSM

The magnetic properties of pure Fe₃O₄ and doped Fe₃O₄ were investigated by means of vibrating sample magnetometer model number Lakeshore VSM-7410, at room temperature supplied with 10,000 gauss applied a magnetic field. The magnetization curves of pure and doped iron oxide are portrayed in Fig. 5a and b. The obtained data for saturation magnetization (Ms), sensitivity, Coercivity (Hc), Retentivity (Mr) is shown in Table 2. In the Fig. 5a and b the hysteresis loop can be observed for both the materials i.e. pure and doped iron oxides. The saturation magnetization curve for pure Fe₃O₄ is 4.621 emu/g, while the saturation magnetization curve for Co²⁺, Ni²⁺ doped Fe₃O₄ is found to be 209.52 emu/g. The decrease in magnetization value of undoped Fe₃O₄ is can be attributed to the presence of a smaller concentration of weak magnetically contaminated haematite phase. Due to this blended concentration of hematite in undoped Fe₃O₄ the surface of the nanoparticles seems to be inclined or in the other way distorted spins may have repelled the core spins of pure iron oxide leading to align the field direction. Ultimately this results in falling off the saturation magnetization of the undoped iron oxide. While the inflation in the magnetization curves for doped iron oxide is may be due to the addition of dopant concentration of strongly ferromagnetic metals like cobalt and nickel [46].

Table 1

Surface area and particle size calculated using the BET method for spherical particles from SEM data.

Synthesized compound	Calcination Temperature (°C)	Crystallite (grain) Size, D nm (XRD)	Particle size, d nm (SEM)	Specific surface the area in m ² /g
Undoped Fe ₃ O ₄	650	25.26	100	4.25
Doped Fe ₃ O ₄	650	24.36	76.92	6.30

3.7. Zeta potential report

In the majority of chemical reactions surface charge is the predominant factor in deciding the adsorption efficiency of a particular material used as an adsorbent. In the present research surface charge was investigated with the assistance of Particle size analyzer, ZS Malvern 200 UK at neutral pH using water as a dispersant. The iron oxide is magnetic nanoparticles at the same time they bear an amphoteric nature means they can develop positive and negative both type of charges on the surface due to addition and elimination of hydrogen ions on the surface. This can be represented as (Fe(OH)₂ + H⁺ → Fe(OH)₂ H⁺) for protonation. Now during the deprotonation Fe⁺OH + H⁺ → FeO⁻ + H⁺. Thus it can be concluded that the formation of Fe–OH on the surface of magnetite nanoparticles in the aqueous medium. Hence it was essential to know the zeta potential of these colloidal phase magnetic nanoparticles. From the analysis report of undoped Fe₃O₄ and doped Fe₃O₄ nanoparticles the zeta potential was found to be -7.96 mV and -14.8 mV, implies that the variation in zeta potential values effects on the stability of iron oxide nanoparticles in the aqueous media due to the formation of ions with magnetic nanoparticles [47]. Although 30 mV is recognized stability values of zeta potential, if the zeta potential values in the range of 60 mV the value considered as an excellent stability phase in the liquid medium. The zeta potential curves for undoped iron oxide and doped iron oxide are represented in Fig. 15 (Supplementary material File).

3.8. XPS analysis

X-ray photoelectron spectroscopy (XPS) is mostly used technique for the surface analysis as well as the elemental composition of the materials. Particularly XPS is broadly used to categorise the wide range of materials to provide valuable quantitative and chemical state information of the materials being used. In the present study the Co²⁺, Ni²⁺ doped Fe₃O₄ nanocatalyst was investigated by XPS the core level XPS signals for the elements can be demonstrated from XPS data. The survey spectrum of doped iron oxide catalyst has been reported in Fig. 6 [48]. As well as the composition of Co²⁺, Ni²⁺ doped Fe₃O₄ nanocatalyst has been reported in Table 3.

3.9. Photocatalytic activity

The photocatalytic degradation of Carbol Fuchsin dye was carried with the help of Quartz Glass Immersion well photocatalytic reactor equipped with 200-W Mercury vapor lamp, double jacket quartz immersion well, magnetic stirrer and chiller for water circulation, safety cabinet with control panel. The overall changes in dye concentration were recorded with the help of Double beam UV-spectrophotometer Jasco-UV 730 in the range of 300–800 nm. The pH of the photocatalytic experiment was recorded with the assist of digital pH meter make Lab India equipped with a glass electrode. The pH meter was previously standardized with the help of buffer capsules of pH 4, 7, 9, 12 ranging from acidic to the basic condition [49].

The photocatalytic degradation of Carbol Fuchsin dye was calculated using the following Eq. (1)

$$\% D = \frac{(C_0 - C_t)}{C_0} \times 100 \quad (1)$$

C₀ is initial concentration and C_t is the concentration at time t.

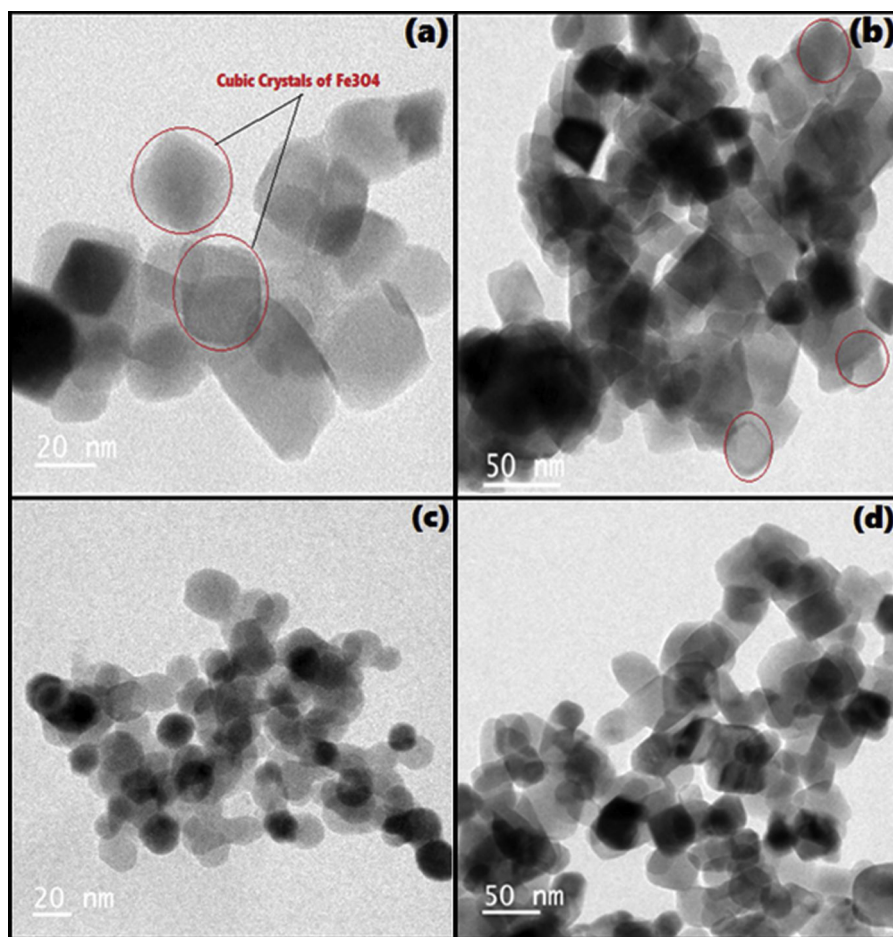


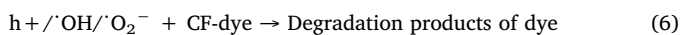
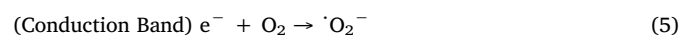
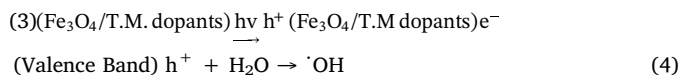
Fig. 4. (a),(b) HR-TEM images of undoped Fe₃O₄ nanoparticles. (c), (d). HR-TEM image of Co²⁺, Ni²⁺ doped Fe₃O₄ nanoparticles.

The specific surface area of undoped Fe₃O₄ and doped Fe₃O₄ nanoparticles was calculated using BET method for spherical particles using the following Eq. (2)

$$S_w = 6/\rho \times d \quad (2)$$

S_w = Surface area, 6 (six) = constant, ρ is the composite density of the materials, d = average particle size of functioning material.

3.9.1. Photocatalytic degradation mechanism of Carbol Fuchsin (CF) dye



3.10. Optimization of parameters

Photocatalytic removal of Carbol Fuchsin (CF) dye was carried out at $\lambda_{\text{max}} 551 \text{ nm}$. The ideal conditions for the removal of dye are found to be 20 ppm dye concentration, pH = 8, undoped and doped Fe₃O₄ catalyst dose 8 g/L. The graphical presentation of the results obtained during the photocatalytic study of CF dye over the undoped and doped Fe₃O₄ catalyst is summarized in Figs. 7–12. The common chemical properties of CF dye are represented in Table 4.

3.11. Effect of catalyst dose

The major role in the effective degradation of dyes played by the amount of catalyst. Thus catalyst dose optimization is a very crucial step in photocatalysis. Here the catalyst dose was monitored from 2 to 8 g/L in a series of the batch experiment after the elaboration of other experimental parameters. At every increment of catalyst dose from 2 to 8 g/L the degradation of Carbol Fuchsin dye was also found to be increased from 81 to 97 % in case of doped iron oxide, while for undoped iron oxide the degradation found to be slightly dropped from 76 to 90 % for 2–8 g/L of catalyst dose respectively. The enhancement of the catalyst does generate the number of sprightly sites of catalyst, which in turn responsible for the effective degradation of Carbol Fuchsin dye. In case of doped iron oxide, the band gap has reduced to 2.5 eV and hence ease of electron transfer from the valence band to the conduction band is a very rapid process to form positive holes and electron at conduction band. Thus positive holes react with water to form hydroxyl radicals while electron in the conduction band interacts with dissolve Dioxygen to form superoxide radicals and hence the dye present on the surface ultimately degraded at the faster rate in comparison to the undoped iron oxide [50,51]. The comparative graph for undoped and doped iron oxide for the effect of catalyst dose is as represented in Fig. 7a and b.

3.12. pH optimization

Most of the catalytical activities are pH dependent hence its optimization is a necessary step in photocatalytic studies. During the photocatalytic degradation of Carbol Fuchsin dye degradation was

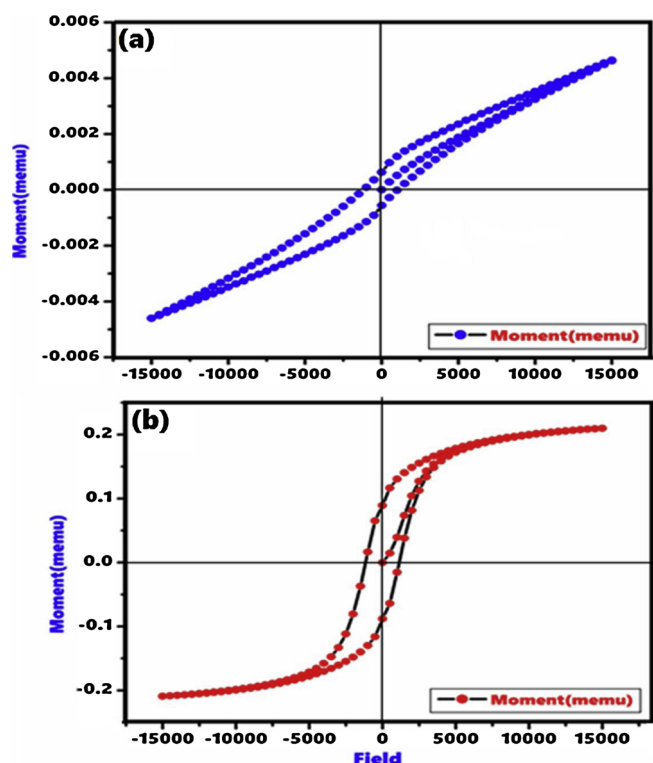


Fig. 5. (a) Magnetization curve of undoped Fe_3O_4 nanoparticles, (b) Magnetization curve of Co^{2+} , Ni^{2+} doped Fe_3O_4 nanoparticles.

examined at the varied values of pH from 1–12. Here the catalyst dose was fixed at 8 g/L, while the concentration of Carbol Fuchsin dye was maintained at 2 mg/L. In the overall photocatalytic degradation study of Carbol Fuchsin dye using undoped and Co^{2+} , Ni^{2+} doped iron oxide it was perceived that the cumulative rate of photocatalytic degradation of CF dye was increased from pH 1 to 8 for both the doped and undoped iron oxide catalyst. After crossing the pH value 8 the rate of photocatalysis on CF dye using doped and undoped iron oxide catalyst was diminished. During this effect pH_{PZC} for both doped and undoped Iron oxide catalyst was monitored for 24 h from pH 1–12, to get the correct pH_{PZC} value, in the present investigation the pH_{PZC} value was found to be 8. The catalyst surface has net zero charges at pH_{PZC} and at $\text{pH} > \text{pH}_{\text{PZC}}$ the surface catalyst is negatively charged while $\text{pH} < \text{pH}_{\text{PZC}}$ surface is positively charged. The catalyst surface becomes negatively charged after pH 8.0 and CF dye turned into additionally anionic shape, therefore, there was sturdy repulsion located among the dye molecule and catalyst surface [52–54]. Consequently, the rate of decay decreases for each undoped and doped iron oxide nanocatalyst after pH 8.0. The effect of pH on CF dye using undoped and doped iron oxide catalyst is as shown in Fig. 8.

3.13. Effect of contact time

The effect of contact time in Photocatalytic/Adsorption investigation is the foremost parameter as it impersonates the effect of catalyst to decompose/degrade the dye. The consequence of contact time on the degradation of Carbol Fuchsin by undoped and doped iron oxide

Table 2
Magnetic properties of pure Fe_3O_4 and Co^{2+} , Ni^{2+} doped Fe_3O_4 nanoparticles.

Entry Number	Compound	Crystallite Size (nm)	Saturation Magnetization Ms (emu/g)	Sensitivity emu	Coercivity Hc (G)	Retentivity Mr(emu/g)
1	Undoped Fe_3O_4	25.26	4.621	–4.800	1110.3	594.11
2	Doped Fe_3O_4	24.36	209.52	–4.800	1149.0	88.60

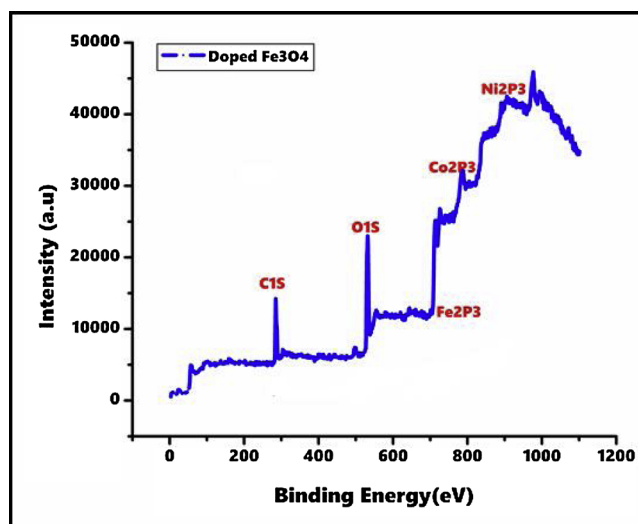


Fig. 6. XPS Survey Spectrum for Co^{2+} , Ni^{2+} doped Fe_3O_4 Nanoparticles.

Table 3

The element composition of Co^{2+} , Ni^{2+} doped Fe_3O_4 from XPS Data.

Element (Atomic %)	O 1s	Fe 2P3	Co 2P3	Ni 2P3	
Co^{2+} , Ni^{2+} doped Fe_3O_4	0.733	1.964	2.113	2.309	RSF
Co^{2+} , Ni^{2+} doped Fe_3O_4	39.581	116.214	125.331	137.443	Corrected RSF
Co^{2+} , Ni^{2+} doped Fe_3O_4	62.42	25.52	12.07	0.0	Total

(Fe_3O_4) is expressed in Fig. 9a and b. The dye was found to be degraded very expeditiously in 25 min after that degradation rate was enhanced leisurely and reached to reaction equilibrium after 70 min and degraded completely in 90 min. It can be concluded that at the initial stage the active sites of iron oxide catalyst are more in number, these active catalyst sites are even additional in case doped Fe_3O_4 due to the presence of more metal ion concentration. Thus at the initial time when dye get adsorbed on the catalyst surface the effective interaction between adsorbed dye and catalyst surface promotes the degradation of dye at the faster rate. At this stage degradation rate is maximum, hence the Carbol Fuchsin and Catalyst achieved the equilibrium condition at 70 min, where maximum degradation of dye was achieved. While remaining all concentration of dye was found to be degraded in next 20 min. Thus overall contact time of degradation of Carbol Fuchsin and iron oxide catalyst was 90 min. The trend of degradation for doped iron oxide for 20–80 mg/L concentration of a dye was 95.5–79% respectively [55,56]. While for undoped iron oxide the concentration of 20–80 mg/L dye solution has a degradation rate of 90–76% as presented in Fig. 9b.

3.14. Effect of initial dye concentration

The concentration of the dye is an important aspect for the photocatalytic application as the concentration of dye may alter the degradation rate if it is not optimized for the particular catalyst used in photocatalysis. The degradation rate of CF dye was evaluated by varying the concentration of CF dye from 10 to 100 ppm. When catalyst concentration is fixed the active sites of catalyst are constant and hence

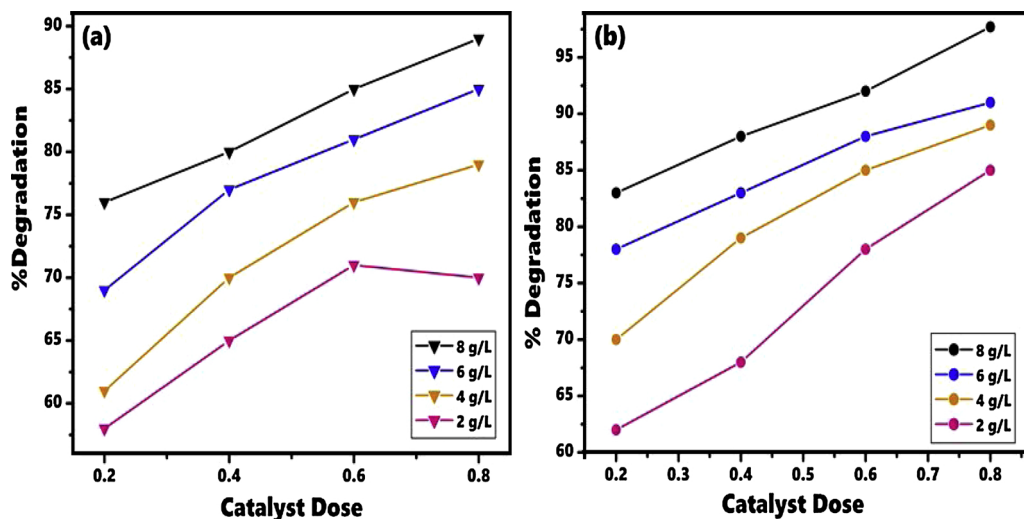


Fig. 7. (a) Effect of undoped Iron oxide catalyst dose on % degradation of Carbol Fuchsin dye for different initial dye concentration with contact time 110 min, pH 8.0. (b) Effect of doped Iron oxide catalyst dose on % degradation of Carbol Fuchsin dye for different initial dye conc. With contact time 110 min, pH 8.0.

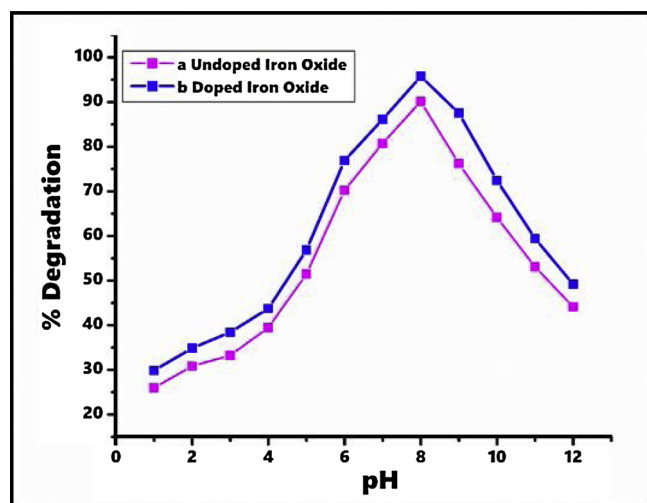


Fig. 8. (a) Effect of pH on degradation of Carbol Fuchsin dye by undoped Iron oxide nanocatalyst. (b). Effect of pH on degradation of Carbol Fuchsin dye by doped Iron oxide nanocatalyst.

it observed in most of the research that degradation of dye is diminished with the multiplication of dye concentration at a fixed amount catalyst. The same trend is observed with the CF dye for undoped and doped iron oxide catalyst, with the series of dye concentration increment the degradation was dropped from 20 ppm to 80 ppm CF dye concentration. During the degradation of CF dye quenching between the excited state molecules of Carbol Fuchsin arise due to irradiation of mercury photons in the presence of a catalyst. The quenching increases with a rise in CF dye concentration, hence with the increment of CF dye concentration the photocatalytic degradation of CF dye solution decreased [57–59]. The effect of dye concentration on photocatalytic performance for undoped iron oxide and doped iron oxide catalyst is as shown in Fig. 10a and b.

3.15. Effect of hydrogen peroxide and dissolved oxygen on the degradation rate of CF

As there is an effective role of Dioxygen in photocatalysis since this dissolved oxygen in combination with e^- forms superoxide radicals. These superoxide radicals further degrade the dye on the catalyst surface. These electrons are transferred from valence band to conduction

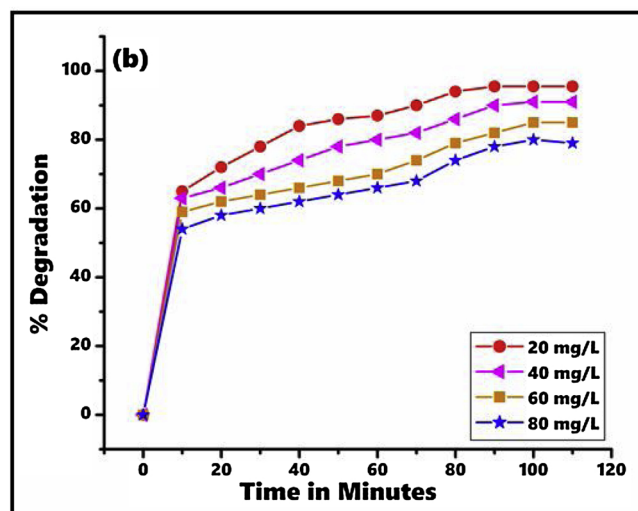
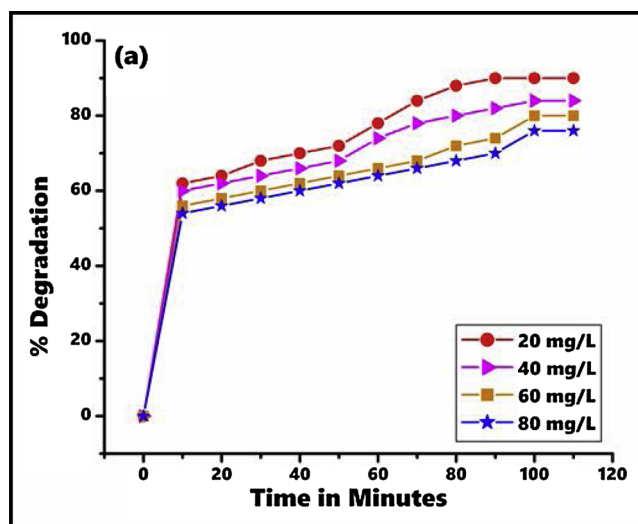


Fig. 9. (a) Effect of contact time on % degradation of Carbol Fuchsin dye for undoped iron oxide catalyst dose 8 g/L at pH 8.0. (b)Effect of contact time on % degradation of Carbol Fuchsin dye at doped iron oxide catalyst dose 8 g/L at pH 8.0.

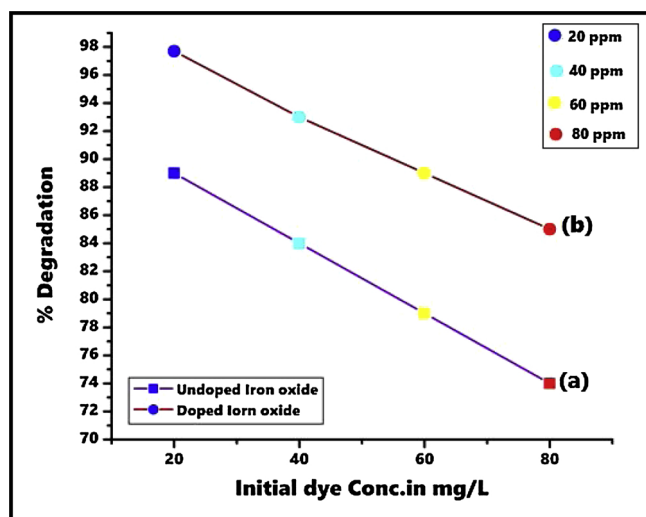


Fig. 10. (a) Effect of initial dye conc. on % degradation of Carbol Fuchsin dye by undoped iron oxide catalyst dose 8 g/L at pH 8.0 (b). Effect of initial dye conc. on % degradation of Carbol Fuchsin dye by doped iron oxide catalyst dose 8 g/L at pH 8.0.

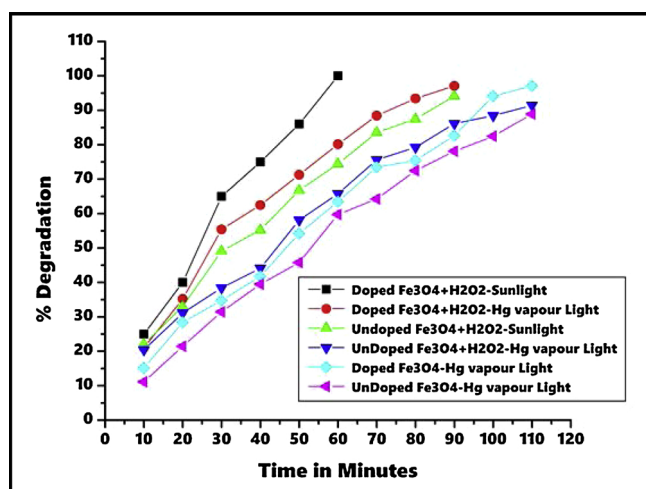


Fig. 11. Photocatalytic Degradation of CF dye using doped and undoped iron oxide catalysed by hydrogen peroxide under sunlight and Hg-Vapour reactor.

band and utilized in the further process which is catalysed due to quanta of photons. Here for an experimental purpose, we carried to set up doped and undoped Fe₃O₄ catalyst, for the photocatalysis was carried in presence of Hg-vapour reactor and conventional sunlight. The optimum reaction conditions were 20 ppm CF dye solution (100 ml), pH 8.0, 0.8 g/100 ml catalyst dose of undoped and doped iron oxide and 30% hydrogen peroxide solution (20 ml). As H₂O₂ in combination with electron forms hydroxide radicals, these hydroxide radicals act as an electron acceptor which is in turn also averts the recombination of (h⁺ / e⁻) pair. Thus it was observed that due to the addition of H₂O₂ in doped iron oxide, and sunlight illumination the CF- dye was found to be degraded almost 99.99% in about 60 min but the same experiment in reactor light illumination degrade 97% of CF dye in 95 min. While for the undoped iron catalyst in combination with H₂O₂ degrade 94% in 90 min under sunlight illumination. In the case of reactor light illumination, in the presence of H₂O₂, the degradation of CF- the dye was achieved in 89% in 110 min [60–62]. The diagrammatic presentation of the experimental results are shown in Fig. 11.

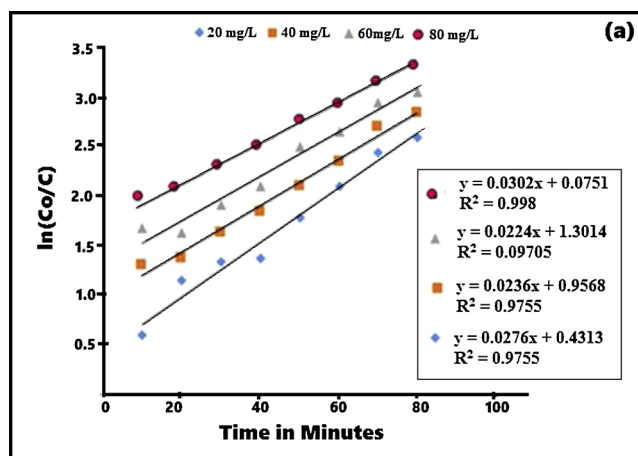


Fig. 12. (a) Pseudo 1st order kinetics for photocatalytic degradation of Carbol Fuchsin dye with undoped Iron oxide (Fe₃O₄) dose 8 gm/L. (b) Pseudo 1st order kinetics for photocatalytic degradation of Carbol Fuchsin dye with doped Iron oxide (Fe₃O₄) dose 8 gm/L.

3.16. Kinetic study for photocatalytic degradation of CF dye

Kinetics study of the photocatalytic experiment is a proficient parameter which can help in determining the order of reactions and other useful chemical parameters of heterogeneous catalysis. The photocatalytic degradation of CF dye at the concise condition over undoped and doped iron oxide (Fe₃O₄) is as shown in Fig. 12 and the kinetics plots are as shown in Fig. 12a and b. For both the catalyst i.e. undoped and doped iron oxide the photocatalysis over CF dye follows the pseudo-first order kinetics. The following Eq. (6) was used for calculation of order kinetics of the reaction.

$$\ln \frac{C_0}{C} = kt \quad (7)$$

Where C and C_0 are the reactant concentration at time $t = t$ and $t = 0$, respectively, k and t are the pseudo-first-order rate constant (reaction rate constant) and time, respectively. The interconnection between $\ln(C/C_0)$ and irradiation time (Reaction time) are as shown in the Fig. 12a and b. It is very conspicuous that there is a linear association between $[\ln(C/C_0)]$ and irradiation time (t). The pseudo-first-order rate constant k and linear regression coefficient (R^2) for CF solutions with different initial CF concentrations are summarized in Table 5.

In keeping with the Langmuir-Hinshelwood version, the truth that the decrease of reaction rate constant with the increase of the initial concentration of CF-dye obtained from Table 5 could be defined as follows. The CF-dye is first of all adsorbed at the surface of undoped and doped iron oxide, and then the photocatalytic degradation takes place

Table 4
The chemical parameters of Carbol Fuchsin dye utilized in the present investigation.

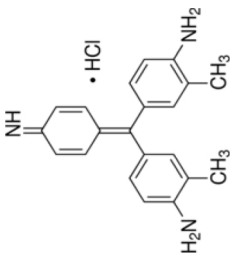
Dye	IUPAC name of the dye	Structure	MW	Molecular Formula	Solubility
Carbol Fuchsin	4-[(4-aminophenyl) (4-iminocyclohexa-2, 5-dien-1-ylidene) methyl]-2-methylaniline hydrochloride		351.87 g/mol	C ₂₁ H ₂₂ ClN ₃	Water (2650 mg/L) at 25 °C

Table 5
Reaction rate constant of CF photocatalytic degradation with different initial concentration for undoped and doped iron oxide catalyst.

Amount of Catalyst	Initial Conc. (mg/L)	The rate constant (K)	R ²
8 gm/L (undoped iron oxide)	20	0.0635	0.9755
	40	0.0544	0.9877
	60	0.0515	0.9705
	80	0.0695	0.9973
8 gm/L (doped iron oxide)	20	0.0601	0.991
	40	0.0527	0.991
	60	0.0506	0.983
	80	0.0488	0.971

underneath Mercury irradiation. With the increase of the initial CF concentrations, the CF-dye molecules congregate on the surface of undoped and doped iron oxide nanocatalysts. However, quenching between these excited molecules irradiated by means of UV light will take place. The quenching probability can also increase with the growth of the initial CF concentrations. Consequently, the photocatalytic efficiency of undoped and doped iron oxide nanocatalyst decreased with the increase of the initial Carbol Fuchsin concentrations.

3.17. Reusability of the undoped and doped Fe₃O₄ catalyst

The steadiness of the undoped and doped iron oxide (Fe₃O₄) catalysts had been pronouncing by way of reusability of the catalysts in the photocatalytic degradation of CF dye in UV-vis illumination. To study its reusability, after photocatalytic degradation the powdered nanocatalyst settled at the base of reaction vessel were collected, filtered via whatman filter paper 40, then the collected nanoparticles were dried and recalcined. The redeem nanoparticles reused for 3 times (three catalytic cycles) in photocatalytic degradation batch of Carbol Fuchsin dye. The reusability batch experiment was performed by maintaining the conditions as the 20 ppm dye concentration, pH = 8, undoped and doped Fe₃O₄ catalyst dose 8 g/L. The degradation percentage of CF dye by utilizing undoped iron oxide after 1st run was 90.42%, 2nd run 89.32%, 3rd run 88.3% and 4th run 87.12%. Whereas expulsion of CF dye by making use of doped iron oxide after 1st run achieved 97%, second run 96.10%, third run 95.3% and 4th run 93.4%. The degradation results of CF dye after reusability are represented in Fig. 13. Thus it can be concluded that the undoped and doped iron oxide catalyst are highly stable for degradation of CF- dye up to four catalytic

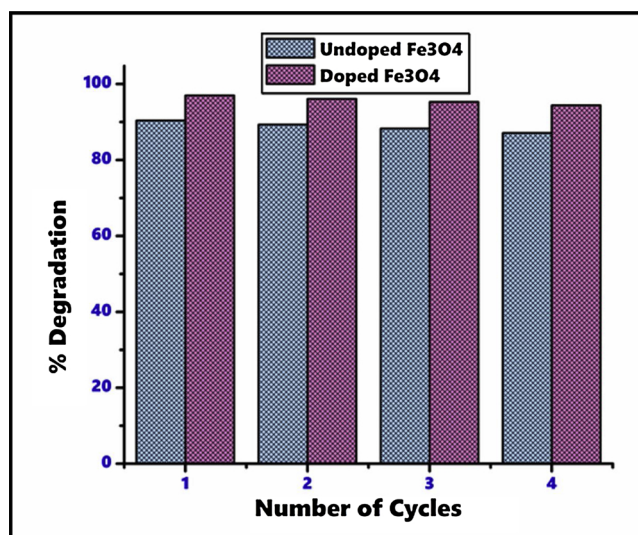


Fig. 13. Recycling Performance of pure and doped iron oxide catalyst for CF dye degradation.

Table 6
Comparative Study using Magnetite (Fe_3O_4) as the catalyst used in the photocatalytic study against different dyes.

Iron-based nanoparticles	Name of the dye/compound	% D	Irradiation time (min.)	Ref.
Fe_3O_4 /PPy	Eosin Y	76.76	70	[37]
	Methyl orange	87.65	80	
	Brilliant green	92.97	90	
$\text{CuO-Fe}_3\text{O}_4$	Desulphurization from Liquid petroleum fuels	93	120	[38]
	Polyaniline- Fe_3O_4	95.2	60	
Fe_3O_4 /BiOBr	Rhodamine B	–	100	[40]
Fe_3O_4 /SiO ₂	Crystal Violet	97.5	–	[41]
Fe_3O_4	Cibacron Red FN-R	85.51	–	[42]
FePc/ Fe_3O_4	Methylene Blue	78	120	[43]
Fe_3O_4	Dye Effluent	–	30	[44]
Undoped Fe_3O_4	Carbol Fuchsin	91.20	110	Present Research
Co^{2+} , Ni^{2+} doped Fe_3O_4	Carbol Fuchsin	97.7	110	

% D = Degradation.

cycles with the negligible degradation percent variation. The decrease in minute percentage of CF-dye degradation for undoped and doped iron oxide catalyst can be attributed to the reduce active sites on catalyst surface as well as dropping percentage of catalyst during the recovery. More ever it can finalized that the catalyst reusability was successful over the CF dye in both undoped and doped iron oxide catalyst.

3.18. Comparison of prepared catalyst

The photocatalytic degradation with the aid of catalysts for many organic dyes, pesticides, toxic substances and colours is very current topic of investigation now a days. However many catalyst have been utilized in this process are highly efficient for the degradation mechanism. In this study we utilized undoped and doped iron oxide catalyst for CF dye degradation, both catalysts are successful to remove CF dye with the average of 90% degradation rate. Here we compared the prepared undoped and doped iron oxide catalyst with some reported dyes degraded with the help of iron oxide catalyst, in most of the cases the magnetic iron oxide catalyst is found to be highly efficient in degradation of organic dyes. The comparison of the present research and reported research for the degradation of various dyes is as represented in Table 6.

4. Conclusions

Carbol Fuchsin dye is one of the fundamental contaminant found in industrial wastewater. It enters the surroundings when released through wastewater and exerts unfavorable outcomes on plants and fauna. The proposed nanoparticles are found to be useful for the wastewater purification. The both synthesized undoped and doped iron oxide (Fe_3O_4) nanocatalysts successfully carried out for the elimination of Carbol Fuchsin dye from an aqueous solution. The synthesized doped iron oxide (Fe_3O_4) nanoparticles having the excellent performance for the degradation of Carbol Fuchsin than undoped Fe_3O_4 because of lower band gap in undoped iron oxide catalyst. The degradation efficiency of both catalysts indicated that the low primary dye concentration and high catalyst dose are more favorable for the degradation procedure. The method obeys the pseudo-first-order kinetics with suitable correlation with linear regression coefficient. The experimental effects of this study shows that the doped Fe_3O_4 oxide catalyst degrades Carbol Fuchsin up to 97% whilst undoped Fe_3O_4 oxide degrade as much as 91%. The MSDS of dye producing industries reviews that Carbol Fuchsin is one the hazardous contaminant with persistent facet effects and subsequently its infection need to be eliminated from wastewater to

conquer the common aspect outcomes on living organisms. These nanocatalyst have superb potentials to be used as water purification media, where the capacity of this fabric can be similarly changed to boom its degradation capacity toward centered compounds.

Declaration of Competing Interest

The authors declare that they have no known competing financial interests or personal relationships that could have appeared to influence the work reported in this paper.

Acknowledgments

Authors are gratefully acknowledged to the SAIF-UDCT, Jalgaon (M.S) for SEM, EDS, DLS, Zeta Potential studies. Authors are thankful to SAIF IIT Bombay for TEM analysis, IIT Madras for VSM results, STIC Cochin University, Kerala for XRD results and IIT Roorkee for XPS results. Authors are very thankful to the Department of chemistry, Pratap College, Amalner, Department of Chemistry, L.V.H. College, Panchavati, Nashik (MAH, India) for providing necessary laboratory facilities.

Appendix A. Supplementary data

Supplementary material related to this article can be found, in the online version, at doi:<https://doi.org/10.1016/j.jece.2019.103373>.

References

- [1] S. Farhadi, F. Manteghi, R. Tondfekr, Removal of Congo red by two new zirconium metal-organic frameworks: kinetics and isotherm study, *Monatshefte für Chemie – Chem. Monthly* (2019), <https://doi.org/10.1007/s00706-018-2329-1>.
- [2] K. Parmentier, S. Vercammen, S. Soetaert, C. Schellekens, Carbon dioxide poisoning: a literature review of an often forgotten cause of intoxication in the emergency department, *Int. J. Emerg. Med.* 10 (2017) 1–4.
- [3] B. Yulianto, G. Gumilar, N.L.W. Septiani, SnO₂ nanostructure as pollutant gas sensors: synthesis, sensing performances, and mechanism, *Adv. Mater. Sci. Eng.* (2015) 1–14.
- [4] P.B. Koli, K.H. Kapadnis, U.G. Deshpande, Nanocrystalline-modified nickel ferrite films: an effective sensor for industrial and environmental gas pollutant detection, *J. Nanostructure Chem.* (2019) 1–16, <https://doi.org/10.1007/s40097-019-0300-2>.
- [5] A. Senthilraj, B. Subash, B. Krishnakumar, D. Rajamanickam, M. Swaminathan, M. Shanthi, Synthesis, characterization and catalytic activity of co-doped Ag–Au–ZnO for MB dye degradation under UV-A light, *Mater. Sci. Semicond. Process.* 22 (2014) 83–91.
- [6] K. Pyrzyńska, Removal of cadmium from wastewaters with low-cost adsorbents, *J. Environ. Chem. Eng.* 7 (2019) 102795, <https://doi.org/10.1016/j.jece.2018.11.040>.
- [7] A. Quarta, R.M. Novais, S. Bettini, M. Iafisco, R.C. Pullar, C. Piccirillo, A sustainable multi-function biomorphic material for pollution remediation or UV absorbent: aerosol assisted preparation of highly porous ZnO-based materials from cork templates, *J. Environ. Chem. Eng.* 7 (2019) 102936, <https://doi.org/10.1016/j.jece.2019.102936>.
- [8] P.B. Koli, K.H. Kapadnis, U.G. Deshpande, Study of physicochemical properties, detection and toxicity study of organic compounds from the effluent of MIDC Thane and GIDC Ankleshwar industrial zone, *Appl. Water Sci.* 8 (2018) 1–9.
- [9] M.R. Patil, V.S. Shrivastava, Adsorptive removal of methylene blue from aqueous solution by polyaniline-nickel ferrite nanocomposite: a kinetic approach, *Desalin. Water Treat.* (2015) 1–9, <https://doi.org/10.1080/19443994.2015.1004594>.
- [10] O.A. Attallah, M.A. Al-Ghobashy, M. Nebsen, M.Y. Salem, Removal of cationic and anionic dyes from aqueous solution with magnetite/pectin and magnetite/silica/pectin hybrid nanocomposites: kinetic, Isotherm and mechanism analysis, *RSC Adv.* 6 (2016) 11461–11480.
- [11] M.R. Patil, V.S. Shrivastava, Adsorption removal of carcinogenic acid violet19 dye from aqueous solution by polyaniline- Fe_3O_4 magnetic nano-composite, *J.Mater.Environ.Sci.* 6 (2015) 11–21.
- [12] Ciara Byrne, G. Subramanian, S.C. Pillai, Recent advances in photocatalysis for environmental applications, *J. Environ. Chem. Eng.* 6 (2018) 3531–3555.
- [13] N.A.H.M. Zaidi, L.B.L. Lim, A. Usman, Enhancing adsorption of malachite green dye using base-modified *Artocarpus odoratissimus* leaves as adsorbents, *Environ. Technol. Innov.* 13 (2019) 211–223.
- [14] D. Venkatesh, S. Pavalamalar, K. Anbalagan, Selective photodegradation on dual dye system by recoverable nano SnO₂ photocatalyst, *J. Inorg. Organomet. Polym. Mater.* 29 (2019) 939–953, <https://doi.org/10.1007/s10904-018-01069-w>.
- [15] S. Kutluay, O. Baytar, O. Sahin, Equilibrium, kinetic and thermodynamic studies for dynamic adsorption of benzene in gas phase onto activated carbon produced from *Elaeagnus angustifolia* Seeds, *J. Environ. Chem. Eng.* 7 (2019), <https://doi.org/10.1016/j.jece.2019.103373>.

- 1016/j.jece.2019.102947.
- [16] D. Dogan, H. Turkdemir, Electrochemical treatment of actual textile Indigo dye effluent, *Pol. J. Environ. Stud.* 21 (2012) 1185–1190.
- [17] E.N. Zare, A. Motahari, M. Sillanpaa, Nano adsorbents based on conducting polymer nanocomposites with main focus on polyaniline and its derivatives for removal of heavy metal ions/dyes: a review, *Environ. Res.* 162 (2018) 173–195.
- [18] H.B. Hadjitaief, M.B. Zinaa, M.E. Galvez, P. Da Costa, Photocatalytic degradation of methyl green dye in aqueous solution over natural clay-supported ZnO-TiO₂ catalysts, *J. Photochem. Photobiol. A: Chem.* 315 (2016) 25–33.
- [19] D. Li, L. Li, W. Guo, Z. Chang, M. Lu, Synthesis and characterization of Mo-Sb-S tri-doped TiO₂ nanoparticles with enhanced visible light photocatalytic activity, *Mater. Sci. Semicond. Process.* 31 (2015) 530–535.
- [20] A. Sepelhi, M.H. Sarrafzadeh, Effect of nitrifiers community on fouling mitigation and nitrification efficiency in a membrane bioreactor, *Chem. Eng. Process. Process. Intensif.* 128 (2018) 10–18.
- [21] Q. Huang, J. Zhao, M. Liu, Y. Li, J. Ruan, Li, J. Tian, X. Zhu, X. Zhang, Y. Wei, Synthesis of polyacrylamide immobilized molybdenum disulfide (MoS₂@PDA@PAM) composites via mussel-inspired chemistry and surface-initiated atom transfer radical polymerization for removal of copper (II) ions, *J. Taiwan Inst. Chem. Eng.* 86 (2018) 174–184.
- [22] Q. Huang, J. Zhao, M. Liu, J. Chen, X. Zhu, T. Wu, J. Tian, Y. Wen, X. Zhang, Yen Wei, Preparation of polyethylene polyamine@tannic acid encapsulated MgAl-layered double hydroxide for the efficient removal of copper (II) ions from aqueous solution, *J. Taiwan Inst. Chem. Eng.* 82 (2018) 92–101.
- [23] Y. Liu, H. Huang, D. Gan, L. Guo, M. Liu, J. Chen, F. Deng, N. Zhou, X. Zhang, Y. Wei, A facile strategy for preparation of magnetic graphene oxide composites and their potential for environmental adsorption, *Ceram. Int.* 44 (2018) 18571–18577.
- [24] X. Zhang, Q. Huang, M. Liu, J. Tian, G. Zeng, Z. Li, K. Wang, Q. Zhang, Q. Wan, F. Deng, Y. Wei, Preparation of amine functionalized carbon nanotubes via a bioinspired strategy and their application in Cu²⁺ removal, *Appl. Surf. Sci.* 343 (2015) 19–27.
- [25] Q. Huang, M. Liu, J. Chen, Q. Wan, J. Tian, L. Huang, R. Jiang, Y. Wen, X. Zhang, Y. Wei, Facile preparation of MoS₂ based polymer composites via mussel inspired chemistry and their high efficiency for removal of organic dyes, *Appl. Surf. Sci.* 419 (2017) 35–44.
- [26] X. Zhang, Q. Huang, F. Deng, H. Huang, Q. Wan, M. Liu, Y. Wei, Mussel-inspired fabrication of functional materials and their environmental applications: progress and prospects, *Appl. Mater. Today* 7 (2017) 222–238.
- [27] G. Zeng, T. Chen, L. Huang, M. Liu, R. Jiang, Q. Wan, Y. Dai, Y. Wen, X. Zhang, Y. Wei, Surface modification and drug delivery applications of MoS₂ nanosheets with polymers through the combination of mussel inspired chemistry and SET-LRP, *J. Taiwan Inst. Chem. Eng.* 82 (2018) 205–221.
- [28] Q. Huang, M. Liu, L. Mao, D. Xu, G. Zeng, H. Huang, R. Jiang, F. Deng, X. Zhang, Y. Wei, Surface functionalized SiO₂ nanoparticles with cationic polymers via the combination of mussel inspired chemistry and surface initiated atom transfer radical polymerization: characterization and enhanced removal of organic dye, *J. Colloid Interface Sci.* 499 (2017) 170–179.
- [29] G. Zeng, X. Liu, M. Liu, Q. Huang, D. Xu, Q. Wan, H. Huang, F. Deng, X. Zhang, Yen Wei, Facile preparation of carbon nanotubes based carboxymethyl chitosan nanocomposites through combination of mussel inspired chemistry and Michael addition reaction: characterization and improved Cu²⁺ removal capability, *J. Taiwan Inst. Chem. Eng.* 68 (2016) 446–454.
- [30] L. Huang, M. Liu, H. Huang, Y. Wen, X. Zhang, Y. Wei, Recent advances and progress on melanin-like materials and their biomedical applications, *Biomacromolecules* 19 (2018) 1858–1868.
- [31] X. Zhang, Y. Shi, M. Liu, F. Deng, G. Zeng, Q. Wan, Y. Wei, Recent progress and development on polymeric nanomaterials for photothermal therapy: a brief overview, *J. Mater. Chem. B* 5 (2017) 194–206.
- [32] M. Liu, J. Ji, X. Zhang, X. Zhang, B. Yang, F. Deng, Z. Li, K. Wang, Y. Yang, Y. Wei, Self-polymerization of dopamine and polyethyleneimine: novel fluorescent organic nanopores for biological imaging applications, *Mater. Chem. B* 3 (2012) 3476–3482.
- [33] Y. Shi, R. Jiang, M. Liu, L. Fu, G. Zeng, Q. Wan, L. Mao, F. Deng, X. Zhang, Y. Wei, Facile synthesis of polymeric fluorescent organic nanoparticles based on the self-polymerization of dopamine for biological imaging, *Mater. Sci. Eng. C* 77 (2017) 972–977.
- [34] M. Liu, G. Zeng, K. Wang, Q. Wan, L. Tao, X. Zhang, Y. Wei, Recent development of polydopamine: an emerged soft matter for surface modification and biomedical applications, *Nanoscale* 8 (2010) 16819–16840.
- [35] X. Zhang, S. Wang, L. Xu, L. Feng, Y. Ji, L. Tao, S. Lia, Y. Wei, Biocompatible Polydopamine fluorescent organic nanoparticles: facile preparation and cell imaging, *Nanoscale* 4 (2012) 5581–5584.
- [36] Y. Liu, K. Ai, L. Lu, Polydopamine and its derivative materials: synthesis and promising applications in energy, environmental, and biomedical fields, *Chem. Rev.* 114 (2014) 5057–5115.
- [37] R.Y. Hong, S.Z. Zhang, G.Q. Di, H.Z. Li, Y. Zheng, J. Ding, D.G. Wei, Preparation, characterization, and application of Fe₃O₄/ZnO core/shell magnetic nanoparticles, *Mater. Res. Bull.* 43 (2008) 2457–2468.
- [38] C. Prasad, S. Gangadhara, P. Venkateswarlu, Bio-inspired green synthesis of Fe₃O₄ magnetic nanoparticles using watermelon rinds and their catalytic activity, *Appl. Nanosci.* 6 (2016) 797–802.
- [39] S. Riaz, M. Bashir, S. Naseem, Iron oxide nanoparticles prepared by modified Co-precipitation method, *IEEE Trans. Magn.* 50 (2014) 1–4.
- [40] H.E. Ghandoor, H.M. Zidan, M.M.H. Khalil, M.I.M. Ismail, Synthesis and some physical properties of magnetite (Fe₃O₄) nanoparticles, *Int. J. Electrochem. Sci.* 7 (2012) 5734–5745.
- [41] V.A.J. Silva, P.L. Andrade, M.P.C. Silva, A. Bustamante D, L.D.L. Valladares, J.A. Aguiar, Synthesis and characterization of Fe₃O₄ nanoparticles coated with fucan polysaccharides, *J. Magn. Magn. Mater.* 343 (2013) 138–143.
- [42] A. Bukowska, W. Bukowski, K. Hus, J. Depciuch, M. Parlińska-Wojtan, Synthesis and characterization of new functionalized polymer-Fe₃O₄ nanocomposite particles, *Express Polym. Lett.* 11 (2017) 2–13.
- [43] B. Babamiri, R. Hallaj, A. Salimi, Ultrasensitive electrochemical luminescence immune sensor for determination of hepatitis B virus surface antigen using CdTe@Cds-PAMAM dendrimer as luminescent labels and Fe₃O₄ nanoparticles as magnetic beads, *Sens. Actuators B Chem.* 254 (2018) 551–560, <https://doi.org/10.1016/j.snb.2017.07.016>.
- [44] A.H. Cahyana, A.I. Reza, Synthesis, and characterization of Fe₃O₄ nanoparticles dispersed in paraffin as solvent, *AIP Conference Proceedings* 2049 (2018), <https://doi.org/10.1063/1.5082452>.
- [45] R. Rahmawati, A. Taufiq, S. Sunaryono, A. Fuad, B. Yulianto, S. Suyatman, D. Kurniadi, Synthesis of magnetite (Fe₃O₄) nanoparticles from Iron sands by Co-precipitation-ultrasonic irradiation methods, *J. Mater. Environ. Sci.* 9 (2018) 155–160.
- [46] Y. Wei, B. Han, X. Hu, Y. Lin, X. Wang, X. Deng, Synthesis of Fe₃O₄ nanoparticles and their magnetic properties, *Procedia Eng.* 27 (2012) 632–637.
- [47] P. Ma, Q. Luo, J. Chen, Y. Gan, J. Du, S. Ding, Z. Xi, X. Yang, Intraperitoneal injection of magnetic Fe₃O₄ - nanoparticle induces hepatic and renal tissue injury via oxidative stress in mice, *Int. J. Nanomedicine* 7 (2012) 4809–4818.
- [48] C. Wang, G. Ma, J. Zhou, M. Zhang, X. Ma, F. Duo, L. Chu, J. Huang, X. Su, Glycine-functionalized Reduced Graphene Oxide for Methylene Blue Removal, (2019), <https://doi.org/10.1002/aoc.5077>.
- [49] P.B. Koli, K.H. Kapadnis, U.G. Deshpande, Fabrication and characterization of pure and modified Co₃O₄ nanocatalyst and their application for photocatalytic degradation of Eosine blue dye: a comparative study, *J. Nanostructure Chem.* 8 (2018) 453–463.
- [50] A.F. Shojaei, A. Shams-Nateri, M. Ghomashpasand, Comparative study of photocatalytic activities of magnetically separable WO₃/TiO₂/Fe₃O₄ nanocomposites and TiO₂, WO₃/TiO₂ and TiO₂/Fe₃O₄ under visible light irradiation, *Superlattices Microstruct.* 88 (2015) 211–224.
- [51] S. Abbasi, M. Hasanpour, The effect of pH on the photocatalytic degradation of methyl orange using decorated ZnO nanoparticles with SnO₂ nanoparticles, *J Mater Sci: Mater Electron.* 28 (2016) 1307–1314.
- [52] K.M. Reza, A.S.W. Kurny, F. Gulshan, Parameters affecting the photocatalytic degradation of dyes using TiO₂: a review, *Appl. Water Sci.* 7 (2017) 1569–1578.
- [53] A. Mohammadi, A.A. Karimi, H.F. Moafi, Adsorption and photocatalytic properties of surface-modified TiO₂ nanoparticles for methyl orange removal from aqueous solutions, *Prog. Color Colorants Coat.* 9 (2016) 247–258.
- [54] B. Malini, G.A. Gnana Raj, C. N and S- doped TiO₂-characterization and Photocatalytic performance for Rose Bengal dye degradation under daylight, *J. Environ. Chem. Eng.* 5 (2018) 5763–5770, <https://doi.org/10.1016/j.jece.2018.09.002>.
- [55] M. Zhang, Z. Yu, H. Yu, Adsorption of Eosin Y, methyl orange and a brilliant green from aqueous solution using Ferro ferric oxide/polypyrrole Magnetic composite, *Polym. Bull.* (2019), <https://doi.org/10.1007/s00289-019-02792-1>.
- [56] S.H. Ammar, Y.S. Kareem, A.D. Ali, Photocatalytic oxidative desulfurization of liquid petroleum fuels using magnetic CuO-Fe₃O₄ nanocomposites, *J. Environ. Chem. Eng.* 6 (2018) 6780–6786, <https://doi.org/10.1016/j.jece.2018.10.031>.
- [57] M.R. Patil, Subhash D. Khairam, V.S. Shrivastava, Synthesis, characterisation of polyaniline-Fe₃O₄ magnetic nanocomposite and its application for removal of an acid violet 19 dye, *Appl. Nanosci.* 6 (2016) 495–502.
- [58] G.S. Cao, G.L. Wang, Y.J. Bai, M.X. Liu, Photocatalytic removal of Rhodamine B using Fe₃O₄/BiOBr magnetic microspheres under visible-light irradiation, *Micro Nano Lett.* 10 (2015) 115–118.
- [59] S. Maleki, F. Falaki, M. Karimi, Synthesis of SDS micelles-coated Fe₃O₄/SiO₂ magnetic nanoparticles as an excellent adsorbent for facile removal and concentration of crystal violet from natural water samples, *J. Nanostruct. Chem.* 9 (2019) 129–139, <https://doi.org/10.1007/s40097-019-0303-z>.
- [60] R. Al-Anbari, A.H. Al-Obaidy, E. Abd, Photocatalytic activity of Fe₃O₄ under solar radiation, *Mesop. Environ. J.* 2 (2016) 41–53.
- [61] K. Wang, L. Yu, S. Yin, H. Li, H. Li, Photocatalytic degradation of methylene blue on magnetically separable FePc/Fe₃O₄ nanocomposite under visible irradiation, *Pure Appl. Chem.* 81 (2009) 2327–2335.
- [62] R. Suriyaprabha, S.H. Khan, B. Pathak, M.H. Fulekar, Spherical surfaced magnetic (Fe₃O₄) nanoparticles as nano adsorbent material for treatment of industrial dye effluents, *Int. J. Nanosci. Nanotechnol.* 13 (2017) 169–175.